Thermal processing and interactions of ethyl formate in model astrophysical ices containing water and ethanol

Article (Accepted Version)

Thermal processing and interactions of ethyl formate in model astrophysical ices containing water and ethanol

Journal:	*ACS Earth and Space Chemistry*
Manuscript ID	sp-2019-00091k.R2
Manuscript Type:	Article
Date Submitted by the Author:	n/a
Complete List of Authors:	Salter, Tara; University of Sussex School of Life Sciences, Chemistry Wootton, Lisa; University of Sussex School of Life Sciences, Chemistry Brown, Wendy; University of Sussex, Chemistry

Thermal processing and interactions of ethyl formate in model astrophysical ices containing water and ethanol

Tara L. Salter, Lisa Wootton and Wendy A. Brown*

Department of Chemistry, School of Life Sciences, University of Sussex, Falmer, Brighton BN1 9QJ, UK

Abstract

Temperature programmed desorption (TPD) and reflection absorption infrared spectroscopy (RAIRS) have been used to investigate the interactions between ethyl formate and water and ethyl formate and ethanol in model astrophysical ices adsorbed on a graphitic model grain surface. Experiments show that the ethyl formate forms hydrogen bonds to both water and ethanol *via* the oxygen lone pairs. This leads to the observation of shifts in the vibrational wavenumber of the C=O and C-O-C modes of ethyl formate, which can potentially be used to identify the environment of this complex organic molecule in astronomical observations. TPD data show that the interaction of ethyl formate with water is stronger than that with ethanol, with an additional species being observed in the TPD spectrum corresponding to the desorption of ethyl formate directly bonded to the water ice surface. The desorption energy of ethyl formate adsorbed on water ice was found to be 48.5 kJ mol^{-1}, compared to 43.2 kJ mol^{-1} for pure ethyl formate monolayers. Ethyl formate also traps in water ice, and undergoes volcano desorption at the water amorphous to crystalline phase transition temperature. In contrast to the water, ethanol has very little effect on the desorption of ethyl formate, with the two species behaving independently even in a co-deposited ice.

Keywords: Temperature programmed desorption; infrared spectroscopy; desorption energy; dust grains; graphite; volcano desorption; amorphous solid water

*Corresponding author: w.a.brown@sussex.ac.uk

Introduction

Complex organic molecules (COMs), are commonly defined as molecules containing carbon and having six or more atoms[1]. Their presence in various astrophysical environments is now well known. For example, COMs have been detected in star forming regions[2], in ices and dust in comets[3–5], in proto-planetary disks[6] and in hot cores such as the Large Magellanic Cloud[7]. Of the detected COMs, esters are thought to be important molecules due to their astrobiological significance as precursors to prebiotic molecules. The simplest ester, methyl formate (CH_3OCHO), has been detected in many low and high-mass star-forming regions[8,9]. The next largest ester, ethyl formate (C_2H_5OCHO), has been detected in the hot dense core Sagittarius B2(N)[10] as well as in Orion[11,12] and in the W51 e2 hot molecular core[13]. Ethyl formate consists of 11 atoms, and is one of the largest COMs that has been unambiguously identified in space. Ethyl formate exists in several different conformations, two of which are shown in Figure 1. The different conformers arise due to rotation within the molecule which gives rise to four possible conformers[14]. The trans conformer was first detected in Sgr B2[10], but subsequent observations have detected both trans and gauche conformers of ethyl formate[11,13]. Although ethyl formate has not yet been detected in cometary ices, methyl formate has been detected on comets Hale-Bopp[15] and Lovejoy[5], therefore it is likely that ethyl formate may also be present in these ices.

Several formation routes of ethyl formate in astrophysical environments have been postulated, either from ethanol or methyl formate. The gas-phase route to the formation of ethyl formate *via* ethanol[16] predicts the abundance of ethyl formate to be one or two orders of magnitude lower than that observed in W51 e2 and SgrB2[13]. In addition, it is also thought that this reaction pathway would be inefficient. More recently, it has been proposed that gas-phase reaction pathways involving the combination of protonated ethanol with formic acid and ammonia could increase the abundance of ethyl formate by more than an order of magnitude[17]. However, massive-star forming regions do not have a high enough abundance of either formic acid or ammonia to efficiently form ethyl formate *via* this route[18]. Hence, models for the formation of ethyl formate based on grain-surface chemistry have been proposed which have predicted abundances in better agreement with the observed values[10]. These models propose that ethyl formate is formed from methyl formate radicals combining with CH_3 radicals, or from ethanol radicals combining with HCO radicals[10].

Given the proposed grain-surface formation routes for ethyl formate, its behaviour on dust grain surfaces and in ices is of interest. However, there have been no previous experimental studies of the surface behaviour of ethyl formate in conditions relevant to astrophysical environments. Previous surface science studies of ethyl formate include temperature programmed desorption (TPD) and reflection absorption infrared spectroscopy (RAIRS) investigations of the adsorption of ethyl formate adsorbed at 86 K on Ni(111) surfaces[19–22]. At the lowest coverages studied, chemisorption is observed, *via* the interaction of the ethyl formate carbonyl lone

pair with the metal surface[21]. Desorption of the monolayer is observed at 136 K in TPD. At higher exposures, TPD data show multilayer desorption at 128 K[19,21]. RAIRS data also show evidence of rotational isomerisation when the exposure is increased from sub-monolayer to multilayer coverages. Chemisorbed ethyl formate forms a s-cis, gauche conformation, as shown in Figure 1. As the exposure is increased, a mixture of different conformations is observed, but at full monolayer coverages, the conformation changes to s-trans, trans. This conformation allows a more closely packed adlayer to form on the surface[20]. This is also the conformation that has been most abundantly observed in star-forming regions[10].

Given the importance of ethanol as a precursor to ethyl formate formation in astrophysical environments, it is expected that ethyl formate will be found in the vicinity of ethanol in space. Hence it is of interest to investigate the behaviour of ethyl formate in the presence of ethanol. Ethanol has been detected in space in the gas and condensed phases in star forming regions[23–27] and in comets[5]. Previous studies have investigated the behaviour of ethanol in model astrophysical ices either as pure ethanol adsorbed on graphite[28–30] or as ethanol in mixed water ices[31].

Water has also been detected in the same star-forming regions as ethyl formate, Sgr B2[32,33] and the Orion nebula[34]. It is therefore expected that ethyl formate may be present in water-dominated icy mantles in these regions. There have been many previous studies of the thermal processing of mixed water ices, illustrating the large effect that water has on the desorption of species present in the ice along with the water[35–37]. In particular, studies have shown that water forms an amorphous structure when adsorbed at low temperature – so called amorphous solid water (ASW)[38]. Two different forms of ASW have previously been investigated, porous amorphous water, which is formed when water is dosed onto a surface at very low temperature (as in the experiments described here), and compact amorphous water, formed by hyperquenching water droplets onto a cold surface[39]. Both have been shown to be relevant to different astrophysical situations[39]. When ASW is heated, a phase transition to crystalline water ice (CI) is observed[38]. Studies have shown that smaller molecules such as CO[40] and CO_2[41] can become trapped in the water ice structure and are then released at the water amorphous to crystalline phase transition (volcano desorption) or when the bulk of the water desorbs from the surface (codesorption). More recent studies have shown that COMs can also become trapped within the water ice structure, depending on their structure and the functional groups that they contain[37]. There are no previous experimental studies of the adsorption and desorption of ethyl formate in the presence of water ice. However, quantum chemical calculations of ethyl formate in water ice predict that its infrared bands will be blue-shifted compared to those of gas-phase ethyl formate[42].

In light of the observation of ethyl formate in various astrophysical environments, and the likelihood that it is found in the presence of ethanol and water ices, we present a detailed RAIRS and TPD study of the behaviour

of ices containing ethyl formate, ethanol and water adsorbed on a carbonaceous model dust grain surface (highly oriented pyrolytic graphite, HOPG). We present data concerning the adsorption and desorption of pure ethyl formate on HOPG, as well as for ethyl formate adsorbed in layered and mixed ices with ASW and ethanol. The thermal processing of these ices has been studied and the interactions of the ethyl formate with the ethanol and ASW ices are investigated. We note that ethyl formate is unlikely to be found in an ice consisting solely of ethyl formate and ethanol in astrophysical environments. However, studying binary ethyl formate/ethanol ices allows a comparison of the hydrogen bonding interactions between ethyl formate and ethanol with those between ethyl formate and water.

Experimental Section

Experiments were performed in an ultra-high vacuum (UHV) chamber with a base pressure of ≤ 2×10^{-10} mbar. The chamber is equipped with a closed cycle helium refrigerator (SHI APD) that allows the sample to be cooled to a base temperature of 30 K. HOPG was used as a model carbonaceous dust grain surface for these experiments. HOPG has previously been shown to be a suitable dust grain analogue for experiments of this type[36]. During experiments, the temperature of the sample was monitored using an E-type thermocouple. The HOPG sample (2 cm × 1 cm × 2 mm) was purchased from Goodfellows Ltd and was exfoliated prior to mounting in the chamber using the Scotch Tape method[43]. The sample was cleaned prior to each experiment by annealing to 250 K. Surface cleanliness was confirmed by the absence of any desorption products in TPD experiments with no dose.

Ethyl formate (> 99.5%, Sigma Aldrich), distilled water and ethanol (99.7%, BDH) were purified prior to dosing into the UHV chamber by repeated freeze-pump-thaw cycles. Model ices were grown on HOPG at base temperature (30 K) *via* background deposition using high precision leak valves. Exposures were recorded in Langmuir (L_m) where 1 L_m = 10^{-6} mbar s. Experiments were undertaken to investigate the adsorption and thermal processing of model ices consisting of pure ethyl formate dosed on HOPG; ethyl formate deposited on top of or mixed with ASW; and ethyl formate deposited on top of or mixed with ethanol. Mixed ices were dosed by admitting the two ice components into the vacuum chamber simultaneously. Mixed ice compositions were determined using the mass spectrometer during dosing. The water ice grown here at 30 K by background dosing is expected to be highly porous, as previously shown[44]. Whilst the experimental methods used here do not allow a direct measurement of the porosity of the ASW, the same growth conditions are used for all experiments to ensure that results can be compared.

Pure ethyl formate experiments were performed for doses ranging from 0.5 – 150 L_m of ethyl formate, corresponding to ice thicknesses of 0.02 – 7.12 nm. For the layered ices, ethyl formate was deposited on top

of 50 L_m of ASW (corresponding to a thickness of 5.36 nm) or 50 L_m of ethanol (a thickness of 3.02 nm). In the mixed ices, a fixed amount of ASW or ethanol was dosed (50 L_m), and the amount of ethyl formate was varied to change the composition of the mixed ice.

TPD experiments were carried out with a Hiden HAL301/PIC mass spectrometer, with a linear heating rate of 0.50 ± 0.01 K s^{-1} regulated by a Eurotherm 2408 interface. For ethyl formate, the most intense mass fragment (m/z = 31) was monitored, apart from in experiments where ethanol was also present. Ethanol also has a mass 31 desorption fragment and hence in these experiments the parent ions for ethyl formate (m/z = 74) and ethanol (m/z = 46) were monitored instead.

RAIRS experiments were performed using a Thermo Nicolet fourier transform infrared spectrometer coupled to a liquid nitrogen cooled mercury-cadmum-telluride detector. Spectra were recorded with a resolution of 4 cm^{-1} and comprise the co-addition of 256 scans. RAIRS annealing experiments were carried out by raising the sample to the target temperature, holding for 3 minutes and then allowing the sample to cool to base temperature (30 K) before recording an infrared spectrum. All experiments were repeated multiple times to ensure reproducibility.

Results and discussion

Pure ethyl formate adsorption on HOPG

Initial experiments focused on studying the adsorption and desorption of ethyl formate on bare HOPG at 30 K. Whilst this ice configuration is not directly relevant to astrophysical situations, studies of pure ethyl formate allow an understanding of the physical processes governing the adsorption of this molecule that can be applied to studies of the interaction of ethyl formate with water and ethanol ice. TPD data for ethyl formate adsorbed on HOPG at 30 K, for exposures of 0.5 to 150 L_m, are shown in Figure 2. At the lowest exposure studied, 0.5 L_m, a single broad peak with a desorption temperature of 126 K is observed (Figure 2A). As the exposure increases, the temperature of this peak steadily decreases until it reaches 118 K at 3 L_m (not shown). The peak shape also becomes asymmetric as the exposure is increased, with a steep leading edge and a long trailing edge being observed. As it is the first TPD peak to be observed, this peak is assigned to the desorption of monolayer ethyl formate from HOPG. The ethyl formate is physisorbed on the HOPG surface, as indicated by the relatively low desorption temperature. The broad nature of this peak is assigned to the presence of repulsive interactions between the adsorbed molecules, which leads to a decreasing desorption temperature with increasing coverage on the surface. Similar repulsive interactions have previously been observed for methyl formate adsorbed on HOPG[45] and for benzene and toluene on HOPG at low exposures[46]. When the exposure is further increased to 4 L_m (Figure 2A), the original peak grows in intensity and remains at the same desorption

temperature, 118 K. Simultaneously, a high temperature shoulder, at 122 K, grows into the TPD spectrum, which then goes on to form a distinct peak at 7 L_m. This peak is assigned to the initial growth of a multilayer of ethyl formate on the HOPG surface.

The observation of both monolayer and multilayer peaks in the higher exposure (> 4 L_m) TPD spectra in Figure 2A suggests that the ethyl formate initially wets the HOPG surface, to form a monolayer, before multilayers are formed on top of the first adsorbate layer. The ethyl formate does not form clusters on the HOPG surface, as in that case the multilayer TPD desorption peak would be observed even at the lowest exposures of ethyl formate, as seen for acetic acid adsorbed on HOPG[45]. Indeed the observation of repulsions between the ethyl formate molecules would also suggest that clusters are unlikely to form. Esters such as ethyl formate and methyl formate do not generally hydrogen bond to themselves, but can hydrogen bond to water, as confirmed by TPD and RAIRS studies for binary ethyl formate and water ices (shown later).

At higher exposures of ethyl formate, Figure 2B, a single peak with shared leading edges and increasing desorption temperature is observed. The desorption temperature varies from 125 K at 20 L_m to 128 K at 50 L_m. The observation of shared leading edges suggests that this peak arises due to the desorption of multilayer ethyl formate from HOPG. At exposures of 50 L_m and higher, Figure 2C shows that the multilayer TPD peak becomes more complex, with the shared leading edge becoming a shoulder on a higher temperature peak. Following an exposure of 100 L_m, the low temperature shoulder becomes more intense than the high temperature peak. Both peaks increase in desorption temperature with increasing exposure, with the low and high temperature peaks reaching a maximum of 129 and 131 K, respectively, at 150 L_m. The desorption temperature of the multilayer observed in Figure 2 is in good agreement with that observed for the desorption of multilayer ethyl formate from a Ni(111) surface[19,21]. TPD data for ethyl formate adsorbed on Ni(111) also showed thermal decomposition in the TPD at higher temperatures[19–22]. However, there is no evidence for decomposition in our TPD data, which is unsurprising given that the desorption temperature suggests that the molecule is physisorbed on the HOPG surface.

In order to better understand the complex desorption observed following ethyl formate exposures above 50 L_m, TPD experiments were also carried out for ethyl formate adsorbed on HOPG at an elevated temperature of 100 K. A range of exposures from 30 to 150 L_m was investigated and the resulting TPD spectra are shown in Figure 3. All TPD traces show a single desorption peak, with shared leading edges and an increasing desorption temperature with increasing exposure. The desorption temperature of the TPD peaks seen in Figure 3 is the same as that of the higher temperature desorption peak observed in Figure 2C. This is confirmed by the spectra shown in the inset of Figure 3, which clearly show that only the high temperature TPD peak is observed following the adsorption of 100 L_m of ethyl formate at 100 K.

The observation of two peaks in the TPD spectra seen in Figure 2C and of just the higher temperature peak following adsorption at 100 K (Figure 3) can be assigned to different phase changes of the ethyl formate ice. In fact, RAIRS data (shown later) show that the phase change occurs prior to desorption, following annealing of the ice to 100 K. RAIRS data also show that two different crystalline forms of ethyl formate are formed as a function of temperature, in agreement with previous observations[14]. The previous work was not able to assign the structure of the different crystalline phases of ethyl formate to particular structures, but labelled them as crystalline phases I and II[14]. The initial phase change leads to the conversion of amorphous ethyl formate, adsorbed at 30 K, to a crystalline form of the ice previously labelled crystalline phase II[14]. This assignment is made by comparison of the RAIR spectra from this phase (shown later) with previously recorded infrared spectra[14]. Following adsorption at higher temperature, a different crystalline phase (crystalline phase I[14]) is formed. This same phase is also observed following high temperature annealing of the ethyl formate layer (see later). Further evidence for the formation of two different phases of ethyl formate is shown in Figure 4. Figure 4 shows isothermal desorption data for different exposures of ethyl formate, recorded by holding the temperature of the sample at 120 K and monitoring desorbing gases with the mass spectrometer. The data in Figure 4 clearly show the presence of two different desorption regimes for these ices, with different desorption rates. These two regimes correspond to the desorption of the two crystalline phases of ethyl formate seen in Figure 2C. Figure 4 also shows an isothermal desorption spectrum for 100 L_m of ethyl formate dosed onto HOPG at 100 K. This spectrum shows only one desorption rate, in agreement with the TPD spectra seen in Figure 3.

The two ethyl formate TPD peaks in Figure 2C are therefore assigned to the formation of different crystalline phases of ethyl formate. Phase changes before and during desorption are also seen for the desorption of water ice, where a low temperature shoulder is seen on the main TPD peak, assigned to the amorphous to crystalline phase transition of water ice[47]. Similar effects have also been seen in TPD spectra recorded for the desorption of glycolaldehyde[45] and propan-2-ol[48] from HOPG. Furthermore, phase transitions have also been seen using infrared spectroscopy to study other COMs such as methyl formate[45,49], acetic acid[45,50] and acetonitrile[51]. This assignment of the TPD spectra observed in Figure 2C to the crystallisation of ethyl formate is also confirmed by RAIRS data, shown later.

In order to determine the desorption order, desorption energy and pre-exponential factor for the desorption of ethyl formate from HOPG, quantitative analysis of the TPD data shown in Figures 2 and 3 was performed. The method used has been described previously[36] and has been used successfully to give kinetic parameters for a wide range of different molecules. The desorption energy, order of desorption and pre-exponential factor for ethyl formate monolayer and multilayer coverages are given in Table 1. Also shown in Table 1 is a value for

the desorption of ethyl formate from an ASW surface (discussed later). The errors in the desorption order, as given in Table 1, are determined by evaluating the greatest and least slope of the linear fit to the data used to determine the desorption order[36]. These errors are then carried forward to give the errors in the desorption order and pre-exponential values given in Table 1.

For monolayer ethyl formate desorbing from HOPG, a desorption order of 0.79 ± 0.14 was determined. This agrees with the assignment of the initial TPD peak to monolayer desorption, since monolayer desorption has an expected desorption order of 1. A desorption energy of 43.2 ± 3.0 kJ mol^{-1} and pre-exponential factor of 4.2 x 10^{20} s^{-1} were also determined for the monolayer. This pre-exponential factor is relatively high when compared to expected values for monolayer desorption (usually 10^{13} – 10^{15} s^{-1}). However, ethyl formate is a large, complex, molecule and other studies have previously shown that the value of the pre-exponential factor scales with molecular size[52] due to an increase in entropy gain on desorption.

Table 1. *Kinetic parameters for monolayer and multilayer ethyl formate adsorbed on HOPG at 30 K, multilayer ethyl formate adsorbed on HOPG at 100 K, and monolayer ethyl formate adsorbed on ASW. The values for ethyl formate desorbing from HOPG are obtained using leading edge analysis[36] whilst those for ethyl formate adsorbed on ASW are obtained using a kinetics simulation package (Kinetiscope).*

	Desorption order	**Desorption energy / kJ mol^{-1}**	**Pre-exponential factor**
Monolayer	0.79 ± 0.14	43.2 ± 3.0	$4.2 \times 10^{20 \pm 1.3}$ s^{-1}
Multilayer	0.19 ± 0.03	44.6 ± 1.1	$1.6 \times 10^{30 \pm 0.3}$ molec cm^{-2} s^{-1}
Multilayer adsorbed at 100 K	0.09 ± 0.03	46.5 ± 0.7	$3.5 \times 10^{32 \pm 0.2}$ molec cm^{-2} s^{-1}
Monolayer on ASW	1 ± 0.1	48.5 ± 2.0	$10^{16 \pm 1}$ s^{-1}

The desorption order for multilayer ethyl formate, as shown in Table 1, is 0.19 ± 0.03. This confirms the assignment of this peak in the TPD spectrum to the desorption of a multilayer species, since multilayer desorption typically shows zero order desorption. The pre-exponential factor for the desorption of the ethyl formate multilayer is considerably larger than that for the monolayer (Table 1), as expected for a multilayer species[36]. The multilayer pre-exponential value is in good agreement with that previously determined for the desorption of methyl formate multilayers from HOPG (8×10^{29} molec cm^{-2} s^{-1})[45].

Table 1 shows that multilayer ethyl formate desorption has a slightly higher desorption energy than the monolayer desorption, as to be expected from the slightly higher desorption temperature. The desorption

energy for crystalline multilayer ethyl formate adsorbed at 100 K is 46.5 ± 0.7 kJ mol^{-1}, compared to 44.6 ± 1.1 kJ mol^{-1} for the desorption of crystalline multilayer ethyl formate formed after annealing a layer adsorbed at 30 K (Table 1). It is common for different ice structures and phases to have different desorption energies. For example, a similar effect has also been seen for amorphous and crystalline propan-2-ol[48], where the crystalline multilayer ice had a desorption energy around 3 kJ mol^{-1} higher than that for the amorphous ice. There are no other literature values of the desorption energy of ethyl formate, however this value is reasonable for the desorption of a large, complex, organic molecule. The desorption energy for ethyl formate is, as expected, larger than that of the smaller ester methyl formate (35 kJ mol^{-1} for the multilayer) adsorbed on HOPG[45], due to the increased size of the molecule. However, the desorption energy is smaller than that for a strongly hydrogen-bonded species such as ethanol[28,29] or propan-2-ol[48], as expected.

RAIRS investigations were also carried out for ethyl formate adsorbed on HOPG, to determine the structure of ethyl formate and how it changes upon annealing the adlayer. The adsorption and annealing of a range of exposures of ethyl formate on HOPG were investigated. RAIR spectra recorded during the adsorption of ethyl formate at 30 K show a number of infrared bands which increase in intensity with increasing ethyl formate dose (not shown). There are no shifts in the observed bands with increasing exposure, confirming that the ethyl formate is physisorbed on the HOPG surface as seen from the TPD data. Instead, the observed infrared bands are observed to grow in intensity as the amount of ethyl formate on the surface increases. Figure 5 shows selected RAIR spectra for the adsorption and annealing of ethyl formate on HOPG. The top spectrum (A) in Figure 5 shows the RAIR spectrum of 100 L_m ethyl formate adsorbed on HOPG at 30 K. At 30 K, the same bands were observed for all exposures investigated and hence the 100 L_m spectrum is shown as it has a good signal to noise ratio. The RAIR spectrum shown in Figure 5A is in good agreement with that seen previously for the formation of multilayer ethyl formate on Ni(111) [19–22]. The assignments for the infrared bands shown in Figure 5 are made by comparison to the literature[14,19–22,53] and are shown in Table 2. In the high wavenumber region of Figure 5A, only one band is observed at 2995 cm^{-1}. This band is assigned to the asymmetric methyl stretch of ethyl formate. Several bands are also observed in the lower wavenumber region, between 1750 and 800 cm^{-1}. The most intense of these are assigned to the carbonyl (C=O) stretching mode at 1732 cm^{-1} and the C-O-C stretching mode at ~1214 cm^{-1}. Other bands observed are assigned to the methyl rocking modes at 1159 and 1117 cm^{-1}, and to the C-C stretching mode at 1016 cm^{-1}. These observed infrared bands are also in good agreement with those previously observed for ethyl formate in CCl_4[53], futher confirming that the ethyl formate is physisorbed on HOPG.

Table 2. *Infrared peak assignments for ethyl formate adsorbed on HOPG at 30 K, and when annealed to 100 K, and when adsorbed at 100 K. Assignment of the crystalline phases I and II are made by comparison to previous data*[14].

Mode	***Adsorbed on HOPG at 30 K***	***Crystalline phase II – 100 L_m annealed to 100 K***	***Crystalline phase I – adsorbed at 100 K***	***Literature***[20,21]
$\nu_{as}(CH_3)$	2995	2999/2974	2999/2974	
$\nu_{as}(CH_3)$	-	2946	2946	
ν(C=O)	1732	1724/1705	1718	1732
$\delta_{as}(CH_3)$	-	1452/1444	1452/1444	1474/1460
$\delta_s(CH_3)$	-	1385	1383/1377	
CH_2 twist	-	1275	1275	
ν_{as}(C-O-C)	1214-1209	1215/1192	1211/1192	1215
$\rho(CH_3)$	1160	1157	1157	1162
$\rho(CH_3)$	1117	1113	1112	
ν(C-C)	1016	1009	1009	

Infrared experiments were also performed to investigate the thermal processing of the ethyl formate ice, following adsorption on the HOPG surface. For the 100 L_m ethyl formate ice, relatively minor changes are observed in the infrared spectra upon heating to 90 K (not shown). Spectral changes observed include the growth and sharpening of the carbonyl stretch mode at 1732 cm^{-1} and the C-O-C stretching mode shifts from 1214 to 1221 cm^{-1}, whilst also growing in intensity. Following annealing to 100 K, a dramatic change is observed in the RAIR spectrum, as shown in Figure 5B. New bands appear in the spectrum at 1452, 1444, 1385 and 1275 cm^{-1}, which are assigned to the methyl asymmetric deformation and CH_2 twisting modes (see Table 2). Further changes are also observed for other infrared bands: the carbonyl stretching mode at 1732 cm^{-1} splits into two peaks at 1724 and 1705 cm^{-1}; and the C-O-C stretching mode sharpens and splits into two peaks at 1215 and 1192 cm^{-1}, with the high wavenumber band growing in intensity. Changes are also observed for the bands at 1159, 1117 and 1017 cm^{-1} which all show small decreases in their wavenumber values as shown in Table 2. In addition, annealing a 100 L_m ice to 100 K also causes the asymmetric methyl stretch at 2995 cm^{-1} to sharpen and shift to 2999 cm^{-1}, with additional peaks appearing at 2974 and 2946 cm^{-1}. Further annealing leads to further changes in the infrared spectra. Annealing to 115 K leads to the growth of the asymmetric methyl band

at 2999 cm^{-1}. Figure 5C shows that the carbonyl stretching mode decreases in intensity and reduces to one peak at 1722 cm^{-1} following heating to 120 K. The band at 1452 cm^{-1} also increases in strength and the additional bands at 1444 and 1385 cm^{-1}, that appeared following annealing to 100 K, disappear. At the same time, the high wavenumber component of the C-O-C stretching mode at 1215 cm^{-1} reduces in intensity.

RAIR spectra were also recorded for ethyl formate ices adsorbed on HOPG at 100 K. The same infrared bands were observed for a range of exposures from 30 to 150 L_m. Figure 5D shows the RAIR spectrum for 100 L_m of ethyl formate adsorbed at 100 K. This spectrum is similar to that seen for 100 L_m ethyl formate annealed to 120 K (Figure 5C). There are some wavenumber shifts for the 100 K adsorbed layer compared to a layer adsorbed at 30 K and annealed: namely the carbonyl stretching mode is observed at 1718 cm^{-1} for the ice adsorbed at an elevated temperature, compared to 1724 cm^{-1} for the annealed ice; and the C-O-C stretching mode has peaks at 1211 and 1192 cm^{-1} for the ice adsorbed at 100 K, whereas this band shows peaks at 1211 and 1196 cm^{-1} for the ethyl formate ice annealed to 120 K.

There are no previous studies of the annealing of ethyl formate ices adsorbed on surfaces. However, by comparison with infrared spectra observed for other molecules adsorbed on HOPG[28,45,48] and other surfaces[49–51] at low temperature these changes, observed in the infrared spectrum as a result of annealing, can be assigned to structural changes of the ethyl formate ice. Maes *et al*. probed the crystallisation of ethyl formate using infrared and Raman spectroscopy[14]. Two polymorphic forms of crystalline ethyl formate, labelled as phases I and II, were found which gave rise to different vibrational spectra. By comparison with the vibrational spectra recorded by Maes *et al*[14], we assign the contrasting behaviour observed on annealing an ice dosed at low temperature compared to dosing at higher temperature to the formation of two different forms of crystalline ethyl formate. The spectra that are observed following the annealing of ethyl formate ices to 100 K (Figure 5B) are assigned to the formation of so called crystalline ice phase II[14]. In contrast, ethyl formate ices adsorbed at higher temperatures give rise to an infrared spectrum (Figure 5D) which agrees with that previously observed for crystalline phase I[14]. There is no data in the literature that identifies the structure of the two forms of crystalline ethyl formate. It is possible that the different crystalline structures arise due to different ordering in the two structures or due to the presence of different ethyl formate conformers in the crystalline polymorphs.

Interactions of ethyl formate with water and ethanol ices

Binary ices consisting of ethyl formate and either water (in the form of ASW) or ethanol were also investigated in order to determine the interactions between the different ice components. The ices consisted of layers of

ethyl formate (5 to 150 L_m) adsorbed on top of ethanol or water, and mixtures of ethyl formate (9 to 50 L_m) with 50 L_m of water or ethanol.

Figure 6 shows TPD traces for different amounts of ethyl formate adsorbed on, or co-deposited with 50 L_m of ASW at 30 K. The presence of water in the ice clearly affects the desorption and thermal processing of ethyl formate, as expected. Low exposures of ethyl formate (5 L_m) on ASW or co-deposited with ASW clearly show the presence of volcano and co-desorption peaks. The volcano peak is more pronounced for the mixed ice than for the layered ice, as expected due to the mixing of the ice components. An additional peak at 134 K is also observed for the layered ice. This peak is not observed for pure ethyl formate adsorbed on HOPG (Figure 2) or for mixed ethyl formate/ASW ices and can be assigned to the direct bonding of submonolayer ethyl formate to the ASW surface. This same behaviour has also been observed for low exposures of methyl formate on ASW[37]. The direct bonding of the ethyl formate to the water ice surface prevents the observation of repulsions between the ethyl formate molecules, as seen for pure ethyl formate at low exposures (Figure 2A). This is because the stronger bonding of the ethyl formate to the water ice overcomes the repulsive interactions between the ethyl formate molecules.

The desorption energy of the ethyl formate bonded to ASW was determined using the Kinetiscope kinetic simulation package, and the determined parameters are shown in Table 1. Using a desorption order of 1, as expected for monolayer desorption, and a pre-exponential value of 10^{16} s^{-1}, a desorption energy of 48.5 kJ mol^{-1} was found to fit the data well. This value is larger than that determined for the desorption of ethyl formate from HOPG, as expected from the higher desorption temperature seen for this species in TPD. To determine the effect of experimental errors on the Kinetiscope fits, variations in the desorption order, desorption energy and pre-exponential factor of a similar order to those determined from direct analysis of the data for pure ethyl formate (Table 1) were also modelled. The results of including these errors in the Kinetiscope simulation are shown in Figure S1 in the Supplementary information. Errors in the order of desorption, n, give the largest variation in the quality of the Kinetiscope fit, with a change in the desorption temperature of ± 10 K resulting from an error in n of ± 0.1. The best fit to the experimental data is achieved with the parameters given in Table 1.

Figure 6B shows the desorption of a larger exposure of ethyl formate (10 L_m) from layered and mixed ASW ices. Similar behaviour is seen to that observed at lower exposures, with both volcano and co-desorption peaks being observed. For the layered ice, a very broad desorption feature from ~ 120-138 K is also seen. This corresponds to desorption of the ethyl formate from the ASW surface (higher temperature desorption) and to desorption of ethyl formate from the surface of pure ethyl formate (lower temperature desorption). This

behaviour is in good agreement with that previously observed for methyl formate adsorption in the presence of ASW[37].

Figure 6C shows the desorption of a thicker layer of ethyl formate (30 L_m) from the layered and mixed ices. The mixed ice desorption is dominated by volcano desorption, as for other exposures. However the layered ice now shows desorption similar to that observed for the desorption of pure ethyl formate from HOPG, in addition to volcano desorption. Hence the TPD spectrum for the layered ice in Figure 6C can be assigned to the growth of multilayer ethyl formate on top of the ASW. The multilayer desorption peak for the layered ice is smaller than that observed for the same amount of ethyl formate adsorbed directly on HOPG since the ASW surface is very porous and it is only after the pores have been filled that ethyl formate deposits as a multilayer.

The behaviour of ethyl formate in the presence of ASW is entirely in line with that observed for other COMs containing ester, aldehyde or ketone functional groups, as previously described[37]. The ethyl formate clearly interacts with the water ice, as evidenced by the observation of a TPD peak due to the direct binding of ethyl formate to the ASW surface. It is surprising that volcano desorption, resulting from the trapping of ethyl formate in the pores of the ASW structure[54], is observed given the large size of the ethyl formate. Clearly the very porous nature of the ASW allows it to trap even a large COM such as ethyl formate. Similar volcano desorption has been seen in the case other other large COMs such as methyl formate[37], acetone[55] and acetaldehyde[55], and suggests that the molecules can fit into the pores of the ASW, although it is unlikely that they can diffuse through the ASW due to their size.

Further evidence for the relatively strong interactions between ethyl formate and ASW can be seen from the RAIR spectra in Figure 7A. The figure shows RAIR spectra for 10 L_m of ethyl formate adsorbed directly on HOPG and adsorbed in a layered ice on top of ASW. There is clearly a small shift in the C=O vibrational mode, which is seen at 1730 cm^{-1} for the pure ice and at 1727 cm^{-1} for the layered ice. An additional low wavenumber shoulder is also observed on the C=O vibration. By comparison with the RAIR spectrum for the 50% ethyl formate/ASW mixed ice in Figure 7B, this shoulder is assigned to ethyl formate interacting directly with the ASW ice. The mixed ethyl formate/ASW ice in Figure 7B has a C=O vibrational mode at 1716 cm^{-1}. In the mixed ice, ethyl formate and water are completely mixed and hence this C=O vibrational mode at 1712-1716 cm^{-1} provides evidence for the interaction of ethyl formate with the water ice. Given the large shift in the C=O vibrational mode for the mixed ice, it is likely that the ethyl formate forms hydrogen bonds to the ASW *via* the oxygen lone pair on the carbonyl group. The C-O-C vibrational mode is also shifted in the water containing ices compared to the pure ice, giving further evidence for an interaction between the two species. This mode is seen at 1234 and 1236 cm^{-1} in the layered (Figure 7A) and mixed (Figure 7B) ices respectively. Again it is likely that the lone pair on the ester oxygen can form hydrogen bonds to the water ice. This observed shift in the

C=O and C-O-C vibrational modes is larger than that seen for methyl formate[28], suggesting a stronger interaction between ethyl formate and ASW than between methyl formate and ASW.

Additional evidence for a stronger interaction between ASW and ethyl formate compared to ASW and methyl formate can be seen in Figure 8. Figure 8 shows TPD spectra for mixed ethyl formate/ASW ices of various compositions. It is clear that increasing amounts of ethyl formate cause the volcano desorption peak to decrease in temperature (Figure 8A). This observed decrease in volcano desorption temperature arises due to a decrease in the temperature of the ASW-CI phase transition of water ice with increasing amounts of ethyl formate in the mixed ice. This is further demonstrated by the RAIR spectra in Figure 8B which show the OH region for water ice after annealing to 130 K for pure water (top spectrum) and for water in a 50% ethyl formate/ASW ice (bottom spectrum). In the case of the mixed ice, the infrared spectrum looks very different to that of the pure ice annealed to the same temperature[47]. For the mixed ice, the appearance of the infrared spectrum shows that the CI phase transition has already occurred following annealing to 130 K, in contrast to the observations for a pure water ice annealed to 130 K. Clearly the interaction between ethyl formate and ASW has an effect on the water ice, as well as shifting the vibrational modes of ethyl formate.

The effect of ethyl formate on water ice is unexpected when compared to methyl formate, which does not affect water crystallisation[37]. Due to the ester functional groups that ethyl formate contains, it is expected that it will behave as a "complex-intermediate" species as previously predicted[37]. These species are not expected to affect the crystallisation of water ice. However, ethyl formate is a large COM compared to methyl formate. Large molecules exhibit greater physisorption energies due to their increased ability to be polarized, leading to a stronger interaction with the surface. It is hence expected that ethyl formate will show a stronger interaction with the polar ASW surface when compared to smaller COMs such as methyl formate[37], acetaldehyde[55] and acetone[55]. Hence it is not surprising that this stronger interaction therefore affects the ASW-CI phase transition by lowering the temperature of the phase transition.

Figure 9 shows TPD spectra for the desorption of ethyl formate from binary layered and mixed ices consisting of ethyl formate and ethanol. Clearly the interaction between ethyl formate and ethanol is different to that between ethyl formate and ASW. In particular, it is not possible for ethanol to trap ethyl formate in the same way that water does since the phase transition for ethanol occurs prior to desorption[28], in contrast to the water ASW to CI phase transition that occurs during desorption.

Figure 9A shows TPD spectra for 5 L_m of ethyl formate in layered and mixed ices with ethanol. In both cases, the desorption looks very similar to that observed for the desorption of ethyl formate directly adsorbed on HOPG. Indeed, all three TPD curves for the different systems share a leading edge, indicating similar desorption

behaviour. The only difference is that the ethyl formate desorption peak in the binary ices is sharper than that for the pure ethyl formate ice. This most likely arises due to the lack of repulsion between the ethyl formate molecules adsorbed on top of the ethanol ice, as also observed for adsorption on ASW. It is not clear why the adsorption of ethyl formate is no longer repulsive when it adsorbs on ethanol. However, this effect may arise as a result of the reduced ability of an ethanol surface to polarise the ethyl formate molecule compared to when it is adsorbed on HOPG. Previous work[46,56] has observed repulsive adsorption for benzene on HOPG which was assigned to the polarization of the molecule by the HOPG surface. It is therefore possible that a similar effect could be seen for a large molecule such as ethyl formate. Despite the loss of the repulsive behaviour of ethyl formate, Figure 9A shows that the ethyl formate desorption is relatively unaffected by the presence of ethanol in the ice. This is particularly surprising for the mixed ices where the two components of the ice behave independently of one another.

For 10 L_m of ethyl formate in a layered or mixed ice with ethanol, two peaks are seen in the TPD spectrum in Figure 9B. The higher temperature peak corresponds to the multilayer peak seen for the desorption of pure ethyl formate. The lower temperature peak, seen for both configurations of binary ice, occurs at the same temperature as the peak seen for 5 L_m of ethyl formate desorbing from the binary ices (Figure 9A). Hence the lower temperature peak can be assigned to the desorption of an ethyl formate monolayer species. Again, this is a surprising observation for the mixed ice since it indicates that the ethyl formate and ethanol are desorbing independently of one another. Further confirmation of this assignment of the two peaks observed for the binary ices in Figure 9B to the desorption of monolayer (low temperature peak) and multilayer (higher temperature peak) ethyl formate comes from a comparison with the pure ethyl formate data in Figure 2A. The 7 L_m TPD spectrum in Figure 2A looks very similar to that observed for 10 L_m of ethyl formate adsorbed on or with ethanol (Figure 9B). The only difference in the two sets of TPD spectra is the exposure at which multilayer ethyl formate is first observed. The HOPG surface (Figure 2A) is a flat and well defined surface, whereas the ethanol ice is a relatively heterogeneous surface with a larger surface area. Indeed, experiments show that ethanol initially adsorbs on HOPG in an amorphous (ie heterogeneous) state and it is only as the ice is heated that a more ordered crystalline ethanol layer is formed[28]. Hence the growth of a multilayer is observed at a lower exposure for ethyl formate adsorbed on HOPG than it is for ethyl formate adsorbed on ethanol.

Figure 9C shows TPD spectra for the desorption of 30 L_m of ethyl formate from layered and mixed binary ices. It is clear that the ethyl formate desorption is the same for all ice configurations, indicating that the ethanol has no effect on the ethyl formate at the higher exposures. The data in Figure 9 taken together show that ethyl formate and ethanol behave similarly in the binary ices and in the pure ices in TPD. This is surprising given that

ethanol, like water, has the ability to form hydrogen bonds with polar species. However, the reduced polarity of the ethanol compared to water clearly inhibits the ability of ethyl formate to interact strongly with ethanol.

In contrast to the TPD data, RAIRS data for the ethyl formate/ethanol mixtures (Figure 7) show some evidence of an interaction between the ethyl formate and ethanol. The C=O band of ethyl formate in a 50% mixture with ethanol occurs at 1726 cm^{-1}, compared to 1732 cm^{-1} for pure ethyl formate and 1716 cm^{-1} for ethyl formate in a 50% mixture with ASW (Figure 7B). Additionally, for a thin layer of ethyl formate (10 L_m) adsorbed on 50 L_m of ethanol (Figure S2, supporting information), although the C=O stretch appears at a similar vibrational wavenumber to that seen for pure ethyl formate (1730 cm^{-1}), the C-O-C vibration occurs at 1203 cm^{-1} (Figure S2). This is shifted by 8 cm^{-1} compared to that observed for pure ethyl formate ice. This suggests a weaker interaction between the ethyl formate and ethanol than between ethyl formate and water. Given the observed shift in the C-O-C vibration and the minor shift in the C=O vibration, it is expected that ethyl formate interacts with ethanol *via* the lone pairs on the two oxygen atoms, as it does with water. Similar interactions have previously been seen for acetonitrile with ethanol[57].

Annealing the ethyl formate/ethanol mixture to higher temperatures does not lead to crystallisation of the ethyl formate ice, as expected given the mixing in the ice (Figure S3). However, annealing 50 L_m of ethyl formate adsorbed on top of a layer of ethanol does lead to crystallisation to the same phase as initially seen when pure ethyl formate is heated to 100 K, as seen in Figure S3 in the supplementary information. This crystalline phase of ethyl formate was previously assigned to the formation of crystalline phase II[14]. Further heating of the ethyl formate layer adsorbed on top of ethanol does not lead to any further phase change, in contrast to observations for pure ethyl formate. Hence the underlying layer of ethanol clearly inhibits the transformation of ethyl formate into the higher temperature crystalline phase.

Conclusions and astrophysical implications

Ethyl formate has been detected in space in environments where water is also present[32–34]. Models for the formation of ethyl formate have also focused on grain-surface chemistry, with ethyl formate being formed from either methyl formate or ethanol[10]. Hence, we have undertaken a detailed TPD and RAIRS investigation of the interactions between ethyl formate and water and ethyl formate and ethanol in model interstellar ices grown on an HOPG surface. The aim of these investigations was to understand how ethyl formate interacts with these two species in astrophysical environments. The water ice investigated here is highly porous, as compared to more compact ASW investigated in other studies[39]. Porous water ice allows the investigation, in detail, of the interactions between ethyl formate and the ASW surface. It also allows the study of the trapping and diffusion of molecules in water ice, both of which have been shown to be important in different

astrophysical environments[35, 58]. Trapping of molecules within the pores of water ice occurs during the compaction of porous ASW to compact ASW, and hence understanding the trapping of molecules within the pores of water ice can help us to understand the way in which astrophysical ices desorb when heated[35, 58]. Both porous and amorphous forms of ASW are found in different astrophysical environments[39], depending on the processing that takes place prior to desorption of the ice. However, it is noted that the results described above, and hence the astrophysical implications described here, are most relevant to environments where porous amorphous water is found and where the formation of ethyl formate takes place prior to compaction of the porous ASW.

Ethyl formate is an ester. It is a large polar molecule which has lone pairs on both the carbonyl and ester oxygen atoms. Ethyl formate is not able to form intermolecular hydrogen bonds, however the lone pairs on the two oxygen atoms allow it to form hydrogen bonds with other species. Given the ability of water and ethanol to hydrogen bond, it is therefore expected that a relatively strong interaction may occur between ethyl formate and ethanol or water.

Our results show that ethyl formate can form hydrogen bonds to both water and ethanol. The hydrogen bonds formed with water have a larger effect on the ethyl formate molecule than those formed with ethanol. This particularly manifests itself in TPD spectra, where there is an additional desorption peak seen for ethyl formate/water layered and mixed ices that can be assigned to the desorption of ethyl formate bonded directly to water. This desorbing species has a desorption energy of 48.5 kJ mol^{-1}, compared to 43.2 kJ mol^{-1} for the desorption of pure monolayer ethyl formate. In contrast, no additional desorption features are seen for ethyl formate adsorbed in either layered or mixed ices with ethanol. In addition to this new desorption feature, water also affects the desorption behaviour of ethyl formate by trapping it in the pores of the water ice as the water undergoes a phase change. This manifests itself in the TPD spectra by the observation of volcano and codesorption peaks for ethyl formate. The result of this is that the bulk of the ethyl formate remains on the surface for longer than it would if it were present as a pure ice.

TPD spectra recorded for ethyl formate and ethanol binary ices show little effect of the ethanol on the ethyl formate. The two species behave independently of one another, and desorb as if the other species is not present in the ice. The only effect that ethanol has on the adsorption of ethyl formate is that it prevents repulsions occurring between the ethyl formate molecules, observed for the adsorption of pure ethyl formate at the lowest exposures.

Given the relatively strong effect that water has on the desorption of ethyl formate, it is expected that this will manifest itself in astrophysical environments where ethyl formate is found in the presence of porous water

ice. In particular, the desorption behaviour of ethyl formate will be influenced by the water. It is therefore necessary to take account of this in any models that detail thermal desorption of ethyl formate, such as hot core models. Previously, an attempt has been made to classify astrophysical molecules according to their desorption properties, thus allowing a description of general classes of desorption to be incorporated into astrophysical models[35,58]. More recently, this classification has been extended to C, H, and O containing COMs[37]. Using our previous classification for COMs, ethyl formate can be classified as a complex intermediate species, as previously predicted[37]. This means that is is a polar species that is expected to show mainly volcano desorption, with a small amount of codesorption. Molecules of this type, as seen for ethyl formate, also show an additional desorption event due to a direct interaction with water ice. In contrast to smaller COMS such as methyl formate, ethyl formate is also shown to have an effect on the crystallisation of water ice with the phase transition temperature being lowered compared to that for pure water. The effect that the behaviour of ethyl formate will have on hot core models will manifest itself in a similar way to the effect observed for methyl formate[37]. Hence ethyl formate will likely be seen in the gas phase at earlier times (lower temperatures) than some other COMs, due to the presence of the low temperature desorption feature assigned to the direct interaction of ethyl formate with the water ice surface. This will potentially lead to its detection earlier than some other COMs and may explain why it has been detected in several astrophysical environments, despite its low abundance.

The RAIR spectra recorded as part of the study described here also show evidence for direct interactions between ethyl formate and water and ethyl formate and ethanol. Shifts are observed in the infrared bands for the C=O and C-O-C vibrational modes of ethyl formate when it is adsorbed in a binary ice with either water or ethanol. In both cases, this suggests the formation of hydrogen bonds between the ethyl formate oxygen lone pairs and the water or ethanol. These hydrogen bonds are stronger in the case of ethyl formate/water ices, as expected due to the more polar nature of the water molecule when compared to ethanol. Laboratory infrared data such as these are useful to aid identification of the environment in which an astrophysically relevant molecule is found, by comparison of observational spectra with data recorded in the laboratory. Comparison of laboratory and observational data has successfully identified the environment in which CO and CO_2 are found in space[59], and hence this same methodology can be applied to the detection of COMs such as ethyl formate in the future. Whilst COMs have not yet been detected in interstellar ices, it is expected that the improved sensitivity and resolution of the James Webb Space Telescope (JWST), expected to launch in 2020, will lead to COM detection in ices. Laboratory infrared data for different composition ices, as recorded here, will hence be essential to aid identification of COMs and the environment in which they are found.

Acknowledgements

This work was undertaken as part of a project funded by the STFC under grant number ST/M000869/1. The STFC are particularly acknowledged for a post-doctoral fellowship for TLS.

Supporting Information

The supporting information provides the following additional figures:

Figure S1 shows the effect of varying the kinetic parameters for the desorption of ethyl formate from the ASW surface within experimental error limits; Figure S2 shows an infrared spectrum for the adsorption of a thin layer (10 L_m) of ethyl formate on ethanol at 30 K; Figure S3 shows infrared spectra for various mixtures and layers of ethyl formate and ethanol annealed to different temperatures.

Figure Captions

Figure 1

The structures of two possible conformers of ethyl formate.

Figure 2

TPD data for varying exposures of ethyl formate adsorbed on HOPG at 30 K. (A) shows exposures from 0.5 – 7 L_m; (B) shows exposures from 10 – 50 L_m; and (C) shows exposures from 60 – 150 L_m.

Figure 3

TPD data for a range of exposures of ethyl formate from 30 to 150 L_m following adsorption on HOPG at 100 K. The inset shows TPD spectra for 100 L_m of ethyl formate adsorbed at base temperature (30 K) and at 100 K.

Figure 4

Isothermal desorption spectra recorded at 120 K for various exposures of ethyl formate adsorbed at 30 K (50, 70 and 100 L_m) and for 100 L_m ethyl formate adsorbed at 100 K.

Figure 5

RAIR spectra of ethyl formate adsorbed on HOPG. (A) shows 100 L_m of ethyl formate adsorbed on HOPG at 30 K; (B) shows 100 L_m of ethyl formate annealed to 100 K;. (C) shows 100 L_m of ethyl formate annealed to 120 K; and (D) shows the spectrum for 100 L_m of ethyl formate adsorbed on HOPG at 100 K.

Figure 6

TPD traces for 5, 10 and 30 L_m of ethyl formate adsorbed on ASW in layered and mixed ices. (A) shows TPD spectra for 5 L_m (9%) of ethyl formate; (B) shows spectra for 10 L_m (17%) of ethyl formate; (C) shows spectra for 30 L_m (38%) of ethyl formate; and (D) shows a TPD spectrum for the desorption of a pure water ice layer adsorbed on HOPG at 30 K for comparison. In all cases the ASW exposure was 50 L_m.

Figure 7

RAIR spectra for various ice configuratiions on HOPG. (A) Shows RAIR spectra for 10 L_m of ethyl formate adsorbed on HOPG at 30 K (top spectrum) and 10 L_m of ethyl formate adsorbed on top of 50 L_m of ASW at 30 K (bottom spectrum). (B) shows spectra for 50 L_m of ethyl formate adsorbed directly onto HOPG at 30 K, and in a 50% mix with ASW and ethanol at 30 K. The bottom spectrum shows a RAIR spectrum for 50 L_m of ethanol adsorbed on HOPG at 30 K.

Figure 8

(A) TPD traces for ethyl formate and ASW mixtures of various compositions. The top spectra show the desorption of ethyl formate and the bottom spectra show the corresponding desorption of water. (B) Shows the O-H region of the RAIR spectrum for pure water adsorbed on HOPG and annealed to 130 K (top spectrum) and for a 50% ethyl fomate/ASW mixture adsorbed at 30 K on HOPG and annealed to 130 K (bottom spectrum).

Figure 9

TPD traces for 5, 10 and 30 L_m of ethyl formate adsorbed on ethanol in layered and mixed ices. (A) shows TPD spectra for 5 L_m (9%) of ethyl formate; (B) shows spectra for 10 L_m (17%) of ethyl formate; (C) shows spectra for 30 L_m (38%) ethyl formate; and (D) shows a TPD spectrum for the desorption of an ethanol ice adsorbed on HOPG at 30 K for comparison. In all cases the ethanol exposure was 50 L_m.

References

(1) Herbst, E.; van Dishoeck, E. F. Complex Organic Interstellar Molecules. *Annu. Rev. Astron. Astrophys.* **2009**, *47* (1), 427–480. https://doi.org/10.1146/annurev-astro-082708-101654.

(2) Soma, T.; Sakai, N.; Watanabe, Y.; Yamamoto, S. Complex Organic Molecules in Taurus Molecular Cloud-1. *Astrophys. J.* **2018**, *854* (2), 116. https://doi.org/10.3847/1538-4357/aaa70c.

(3) Goesmann, F.; Rosenbauer, H.; Bredehoft, J. H.; Cabane, M.; Ehrenfreund, P.; Gautier, T.; Giri, C.; Kruger, H.; Le Roy, L.; MacDermott, A. J.; et al. Organic Compounds on Comet 67P/Churyumov-Gerasimenko Revealed by COSAC Mass Spectrometry. *Science* **2015**, *349* (6247), aab0689. https://doi.org/10.1126/science.aab0689.

(4) Fray, N.; Bardyn, A.; Cottin, H.; Altwegg, K.; Baklouti, D.; Briois, C.; Colangeli, L.; Engrand, C.; Fischer, H.; Glasmachers, A.; et al. High-Molecular-Weight Organic Matter in the Particles of Comet 67P/Churyumov–Gerasimenko. *Nature* **2016**, *538* (7623), 72–74. https://doi.org/10.1038/nature19320.

(5) Biver, N.; Bockelée-Morvan, D.; Moreno, R.; Crovisier, J.; Colom, P.; Lis, D. C.; Sandqvist, A.; Boissier, J.; Despois, D.; Milam, S. N. Ethyl Alcohol and Sugar in Comet C/2014 Q2 (Lovejoy). *Sci. Adv.* **2015**, *1* (9), e1500863. https://doi.org/10.1126/sciadv.1500863.

(6) Walsh, C.; Millar, T. J.; Nomura, H.; Herbst, E.; Weaver, S. W.; Aikawa, Y.; Laas, J. C.; Vasyunin, A. I. Complex Organic Molecules in Protoplanetary Disks. *Astron. Astrophys.* **2014**, *563*, A33. https://doi.org/10.1051/0004-6361/201322446.

(7) Sewiło, M.; Indebetouw, R.; Charnley, S. B.; Zahorecz, S.; Oliveira, J. M.; van Loon, J. T.; Ward, J. L.; Chen, C.-H. R.; Wiseman, J.; Fukui, Y.; et al. The Detection of Hot Cores and Complex Organic Molecules in the Large Magellanic Cloud. *Astrophys. J.* **2018**, *853* (2), L19. https://doi.org/10.3847/2041-8213/aaa079.

(8) Cazaux, S.; Tielens, A. G. G. M.; Ceccarelli, C.; Castets, A.; Wakelam, V.; Caux, E.; Parise, B.; Teyssier, D. The Hot Core around the Low-Mass Protostar IRAS 16293-2422: Scoundrels Rule! *Astrophys. J.* **2003**, *593* (1), L51–L55. https://doi.org/10.1086/378038.

(9) Brown, R. D.; Crofts, J. G.; Godfrey, P. D.; Gardner, F. F.; Robinson, B. J.; Whiteoak, J. B. Discovery of Interstellar Methyl Formate. *Astrophys. J.* **1975**, *197*, L29. https://doi.org/10.1086/181769.

(10) Belloche, A.; Garrod, R. T.; Müller, H. S. P.; Menten, K. M.; Comito, C.; Schilke, P. Increased Complexity in Interstellar Chemistry: Detection and Chemical Modeling of Ethyl Formate and n -Propyl Cyanide in Sagittarius B2(N). *Astron. Astrophys.* **2009**, *499* (1), 215–232. https://doi.org/10.1051/0004-6361/200811550.

(11) Tercero, B.; Kleiner, I.; Cernicharo, J.; Nguyen, H. V. L.; López, A.; Caro, G. M. M. Discovery of Methyl Acetate and Gauche Ethyl Formate in Orion. *Astrophys. J.* **2013**, *770* (1), L13. https://doi.org/10.1088/2041-8205/770/1/L13.

(12) Peng, Y.; Rivilla, V. M.; Zhang, L.; Ge, J. X.; Zhou, B. ALMA Observations of Ethyl Formate toward Orion KL. *Astrophys. J.* **2019**, *871* (2), 251. https://doi.org/10.3847/1538-4357/aafad4.

(13) Rivilla, V. M.; Beltrán, M. T.; Martín-Pintado, J.; Fontani, F.; Caselli, P.; Cesaroni, R. On the Chemical Ladder of Esters. *Astron. Astrophys.* **2017**, *599*, A26. https://doi.org/10.1051/0004-6361/201628823.

(14) Maes, I. I.; Herrebout, W. A.; van der Veken, B. J. Vibrational Conformational Analysis of Ethyl

Formate. *J. Raman Spectrosc.* **1994**, *25* (7–8), 679–691. https://doi.org/10.1002/jrs.1250250731.

(15) Bockelée-Morvan, D.; Lis, D. C.; Wink, J. E.; Despois, D.; Crovisier, J.; Bachiller, R.; Benford, D. J.; Colom, P.; Davies, J. K.; Gérard, E.; et al. *New Molecules Found in Comet C/1995 O1 (Hale-Bopp) Investigating the Link between Cometary and Interstellar Material*; 2000; Vol. 353.

(16) Charnley, S. B.; Kress, M. E.; Tielens, A. G. G. M.; Millar, T. J. Interstellar Alcohols. *Astrophys. J.* **1995**, *448*, 232. https://doi.org/10.1086/175955.

(17) Taquet, V.; Wirström, E. S.; Charnley, S. B. Formation and Recondensation of Complex Organic Molecules During Protostellar Luminosity Outbursts. *Astrophys. J.* **2016**, *821* (1), 46. https://doi.org/10.3847/0004-637X/821/1/46.

(18) Zhang, Q.; Ho, P. T. P. Dynamical Collapse in W51 Massive Cores: NH 3 Observations. *Astrophys. J.* **1997**, *488* (1), 241–257. https://doi.org/10.1086/304667.

(19) Zahidi, E.; Castonguay, M.; McBreen, P. H. Rotational Isomerization of Esters on Ni(111). *J. Phys. Chem.* **1995**, *99* (51), 17906–17916. https://doi.org/10.1021/j100051a016.

(20) Wang, J.; Castonguay, M.; Roy, J.-R.; Zahidi, E.; Mcbreen, P. H. Gauche-Trans Conformational Changes in Ethyl Formate Chemisorbed on Ni(111): Coverage-Dependent RAIRS Spectra. *J. Phys. Chem. B* **1999**, *103* (21), 4382–4386. https://doi.org/10.1021/jp983601+.

(21) Zahidi, E.; Castonguay, M.; McBreen, P. RAIRS and TPD Study of Methyl Formate, Ethyl Formate, and Methyl Acetate on Ni(111). *J. Am. Chem. Soc.* **1994**, *116* (13), 5847–5856. https://doi.org/10.1021/ja00092a040.

(22) Zahidi, E.; Castonguay, M.; McBreen, P. H. Rotational Isomerization in a Chemisorbed Layer: Ethyl Formate on Ni(111). *Chem. Phys. Lett.* **1995**, *236* (1–2), 122–128. https://doi.org/10.1016/0009-2614(95)00178-7.

(23) Millar, T. J.; MacDonald, G. H.; Habing, R. J. The Detection of Hot Ethanol in G34.3+0.15. *Mon. Not. R. Astron. Soc.* **1995**, *273* (1), 25–29. https://doi.org/10.1093/mnras/273.1.25.

(24) Millar, T. J.; Olofsson, H.; Hjalmarson, A.; Brown, P. . The Detection of Ethanol in W51M. *Astron. Astrophys.* **1988**, *205*, L5–L7.

(25) Turner, B. E. A Molecular Line Survey of Sagittarius B2 and Orion-KL from 70 to 115 GHz. II - Analysis of the Data. *Astrophys. J. Suppl. Ser.* **1991**, *76*, 617. https://doi.org/10.1086/191577.

(26) Schriver, A.; Schriver-Mazzuoli, L.; Ehrenfreund, P.; D'Hendecourt, L. One Possible Origin of Ethanol in Interstellar Medium: Photochemistry of Mixed CO_2–C_2H_6 Films at 11K. A FTIR Study. *Chem. Phys.* **2007**, *334* (1–3), 128–137. https://doi.org/10.1016/j.chemphys.2007.02.018.

(27) Öberg, K. I.; Boogert, A. C. A.; Pontoppidan, K. M.; van den Broek, S.; van Dishoeck, E. F.; Bottinelli, S.; Blake, G. A.; Evans, N. J. The Spitzer Ice Legacy:Ice Evolution from Cores to Protostars. *Astrophys. J.* **2011**, *740* (2), 109. https://doi.org/10.1088/0004-637X/740/2/109.

(28) Burke, D. J.; Wolff, A. J.; Edridge, J. L.; Brown, W. A. The Adsorption and Desorption of Ethanol Ices from a Model Grain Surface. *J. Chem. Phys.* **2008**, *128* (10), 1–12. https://doi.org/10.1063/1.2888556.

(29) Smith, R. S.; Matthiesen, J.; Kay, B. D. Desorption Kinetics of Methanol, Ethanol, and Water from Graphene. *J. Phys. Chem. A* **2014**, *118* (37), 8242–8250. https://doi.org/10.1021/jp501038z.

(30) Ulbricht, H.; Zacharia, R.; Cindir, N.; Hertel, T. Thermal Desorption of Gases and Solvents from Graphite and Carbon Nanotube Surfaces. *Carbon N. Y.* **2006**, *44* (14), 2931–2942.

https://doi.org/10.1016/j.carbon.2006.05.040.

(31) Terwisscha Van Scheltinga, J.; Ligterink, N. F. W.; Boogert, A. C. A.; Van Dishoeck, E. F.; Linnartz, H. Astronomy Infrared Spectra of Complex Organic Molecules in Astronomically Relevant Ice Matrices I. Acetaldehyde, Ethanol, and Dimethyl Ether. *Astrophys. A&A* **2018**, *611*, 35. https://doi.org/10.1051/0004-6361/201731998.

(32) Neufeld, D. A.; Ashby, M. L. N.; Bergin, E. A.; Chin, G.; Erickson, N. R.; Goldsmith, P. F.; Harwit, M.; Howe, J. E.; Kleiner, S. C.; Koch, D. G.; et al. Observations of Absorption by Water Vapor toward Sagittarius B2. *Astrophys. J.* **2000**, *539* (2), L111–L113. https://doi.org/10.1086/312853.

(33) Cernicharo, J.; Lim, T.; Cox, P.; González-Alfonso, E.; Caux, E.; Swinyard, B. M.; Martín-Pintado, J.; Baluteau, J. P.; Clegg, P. Widespread Water Vapour Absorption in SgrB2. *Astron. Astrophys.* **1997**, *323*, L25–L28.

(34) Glanz, J. INFRARED ASTRONOMY: A Water Generator in the Orion Nebula. *Science* **1998**, *280* (5362), 378–378. https://doi.org/10.1126/science.280.5362.378.

(35) Collings, M. P.; Anderson, M. A.; Chen, R.; Dever, J. W.; Viti, S.; Williams, D. A.; McCoustra, M. R. S. A Laboratory Survey of the Thermal Desorption of Astrophysically Relevant Molecules. *Mon. Not. R. Astron. Soc.* **2004**, *354* (4), 1133–1140. https://doi.org/10.1111/j.1365-2966.2004.08272.x.

(36) Burke, D. J.; Brown, W. A. Ice in Space: Surface Science Investigations of the Thermal Desorption of Model Interstellar Ices on Dust Grain Analogue Surfaces. *Phys. Chem. Chem. Phys.* **2010**, *12* (23), 5947–5969. https://doi.org/10.1039/b917005g.

(37) Burke, D. J.; Puletti, F.; Woods, P. M.; Viti, S.; Slater, B.; Brown, W. A. Trapping and Desorption of Complex Organic Molecules in Water at 20 K. *J. Chem. Phys.* **2015**, *143* (16), 164704. https://doi.org/10.1063/1.4934264.

(38) Speedy, R. J.; Debenedetti, P. G.; Smith, R. S.; Huang, C.; Kay, B. D. The Evaporation Rate, Free Energy, and Entropy of Amorphous Water at 150 K. *J. Chem. Phys.* **1996**, *105* (1), 240–244. https://doi.org/10.1063/1.471869.

(39) Gálvez, O.; Maté, B.; Herrero, V. J.; Escribano, R. Ammonium and Formate Ions in Interstellar Ice Analogs. *Astrophys. J.* **2010**, *724* (1), 539–545. https://doi.org/10.1088/0004-637X/724/1/539.

(40) Collings, M. P.; Frankland, V. L.; Lasne, J.; Marchione, D.; Rosu-Finsen, a.; McCoustra, M. R. S. Probing Model Interstellar Grain Surfaces with Small Molecules. *Mon. Not. R. Astron. Soc.* **2015**, *449* (2), 1826–1833. https://doi.org/10.1093/mnras/stv425.

(41) Edridge, J. L.; Freimann, K.; Burke, D. J.; Brown, W. A. Surface Science Investigations of the Role of CO_2 in Astrophysical Ices. *Philos. Trans. R. Soc. A Math. Phys. Eng. Sci.* **2013**, *371,* 20110578. https://doi.org/10.1098/rsta.2011.0578.

(42) Naganathappa, M.; Chaudhari, A. Effect of Ionization on Infrared and Electronic Absorption Spectra of Methyl and Ethyl Formate in the Gas Phase and in Astrophysical H_2O Ice: A Computational Study. *J. Phys. Chem. A* **2011**, *115*, 4743–4756. https://doi.org/10.1021/jp112373k.

(43) Wiesendanger, R.; Eng, L.; Hidber, H. R.; Oelhafen, P.; Rosenthaler, L.; Staufer, U.; Guntherodt, H.-J. Local Tunneling Barrier Height Images Obtained With the Scanning Tunneling Microscope. *Surf. Sci.* **1987**, *189/190*, 24–28.

(44) Maté, B.; Rodríguez-Lazcano, Y.; Herrero, V. J. Morphology and Crystallization Kinetics of Compact (HGW) and Porous (ASW) Amorphous Water Ice. *Phys. Chem. Chem. Phys.* **2012**, *14* (30), 10595–

10602. https://doi.org/10.1039/c2cp41597f.

(45) Burke, D. J.; Puletti, F.; Woods, P. M.; Viti, S.; Slater, B.; Brown, W. A. Adsorption and Thermal Processing of Glycolaldehyde, Methyl Formate, and Acetic Acid on Graphite at 20 K. *J. Phys. Chem. A* **2015**, *119* (26), 6837–6849. https://doi.org/10.1021/acs.jpca.5b04010.

(46) Salter, T. L.; Stubbing, J. W.; Brigham, L.; Brown, W. A. A TPD and RAIRS Comparison of the Low Temperature Surface Behavior of Benzene, Toluene, and Xylene on Graphite. *J. Chem. Phys.* **2018**, *149* (16), 164705. https://doi.org/10.1063/1.5051134.

(47) Bolina, A. S.; Wolff, A. J.; Brown, W. A. Reflection Absorption Infrared Spectroscopy and Temperature-Programmed Desorption Studies of the Adsorption and Desorption of Amorphous and Crystalline Water on a Graphite Surface. *J. Phys. Chem. B* **2005**, *109* (35), 16836–16845. https://doi.org/10.1021/jp0528111.

(48) Ayling, S. A.; Burke, D. J.; Salter, T. L.; Brown, W. A. Desorption and Crystallisation of Binary 2-Propanol and Water Ices Adsorbed on Graphite. *RSC Adv.* **2017**, *7,* 51621-51631. https://doi.org/10.1039/c7ra10410c.

(49) Modica, P.; Palumbo, M. E. Formation of Methyl Formate after Cosmic Ion Irradiation of Icy Grain Mantles. *Astron. Astrophys.* **2010**, *519*, A22.

(50) Bahr, S.; Borodin, A.; Ho, O.; Höfft, O.; Kempter, V.; Allouche, A.; Borget, F.; Chiavassa, T. Interaction of Acetic Acid with Solid Water. *J. Phys. Chem. B* **2006**, *110* (17), 8649–8656. https://doi.org/10.1021/jp055980u.

(51) Bertin, M.; Doronin, M.; Fillion, J.-H.; Michaut, X.; Philippe, L.; Lattelais, M.; Markovits, A.; Pauzat, F.; Ellinger, Y.; Guillemin, J.-C. Nitrile versus Isonitrile Adsorption at Interstellar Grains Surfaces. *Astron. Astrophys.* **2017**, *598*, A18. https://doi.org/10.1051/0004-6361/201629394.

(52) Tait, S. L.; Dohnálek, Z.; Campbell, C. T.; Kay, B. D. N-Alkanes on Pt(111) and on C(0001)/Pt(111): Chain Length Dependence of Kinetic Desorption Parameters. *J. Chem. Phys.* **2006**, *125* (23), 234308. https://doi.org/10.1063/1.2400235.

(53) Charles, S. W.; Jones, G. I. L.; Owen, N. L.; Cyvin, S. J.; Cyvin, B. N. The Vibrational Spectra, Rotational Isomerism, Normal Coordinate Analysis and Mean Amplitudes of Ethyl Formate, Ethyl Chloroformate and Ethyl Cyanoform. *J. Mol. Struct.* **1973**, *16* (2), 225–257. https://doi.org/10.1016/0022-2860(73)80064-X.

(54) Kimmel, G. A.; Stevenson, K. P.; Dohnálek, Z.; Smith, R. S.; Kay, B. D. Control of Amorphous Solid Water Morphology Using Molecular Beams. I. Experimental Results. *J. Chem. Phys.* **2001**, *114* (12), 5284–5294. https://doi.org/10.1063/1.1350580.

(55) Lasne, J.; Laffon, C.; Parent, P. Interaction of Acetone, Hydroxyacetone, Acetaldehyde and Benzaldehyde with the Surface of Water Ice and $HNO_3 \cdot 3H_2O$ Ice. *Phys. Chem. Chem. Phys.* **2012**, *14* (2), 697–704. https://doi.org/10.1039/C1CP21707K.

(56) Thrower, J. D.; Collings, M. P.; Rutten, F. J. M.; McCoustra, M. R. S. Thermal Desorption of C_6H_6 from Surfaces of Astrophysical Relevance. *J. Chem. Phys.* **2009**, *131* (24), 244711. https://doi.org/10.1063/1.3267634.

(57) Methikkalam, R. R. J.; Bhuin, R. G.; Ghosh, J.; Sivaraman, B.; Pradeep, T. Interaction of Acetonitrile with Alcohols at Cryogenic Temperatures. *J. Phys. Chem. C* **2017**, *121* (5), 2822–2835. https://doi.org/10.1021/acs.jpcc.6b11483.

(58) Viti, S.; Collings, M. P.; Dever, J. W.; McCoustra, M. R. S.; Williams, D. A. Evaporation of Ices near Massive Stars: Models Based on Laboratory Temperature Programmed Desorption Data. *Mon. Not. R. Astron. Soc.* **2004**, *354* (4), 1141–1145. https://doi.org/10.1111/j.1365-2966.2004.08273.x.

(59) van Broekhuizen, F. A.; Groot, I. M. N.; Fraser, H. J.; van Dishoeck, E. F.; Schlemmer, S. Infrared Spectroscopy of Solid CO–CO_2 Mixtures and Layers. *Astron. Astrophys.* **2006**, *451* (2), 723–731. https://doi.org/10.1051/0004-6361:20052942.

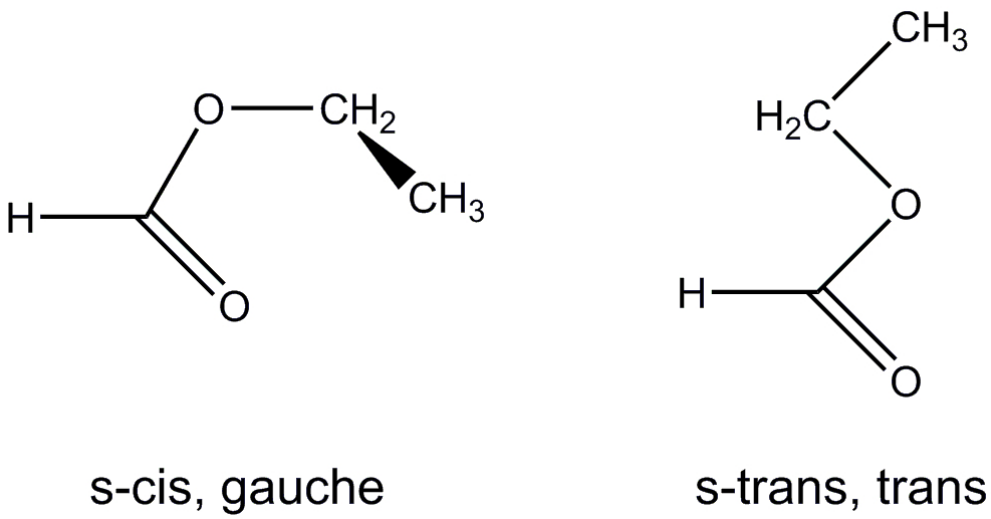

Figure 1: The structures of two possible conformers of ethyl formate.

84x44mm (300 x 300 DPI)

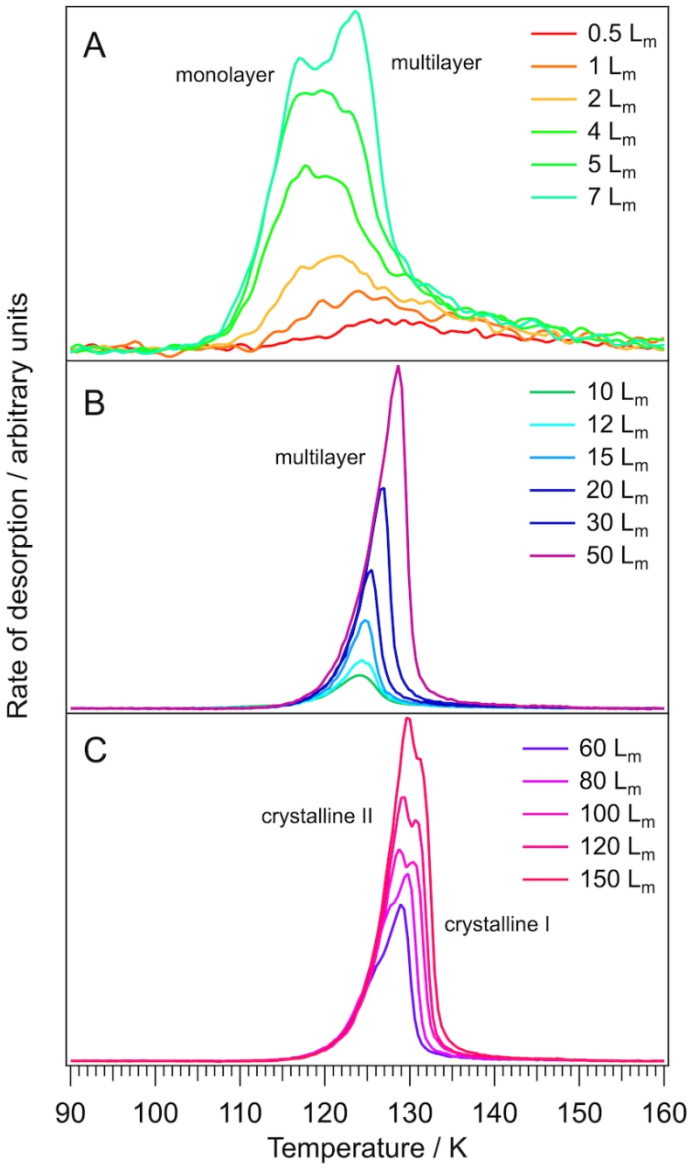

Figure 2: TPD data for varying exposures of ethyl formate adsorbed on HOPG at 30 K. (A) shows exposures from 0.5 – 7 Lm; (B) shows exposures from 10 – 50 Lm; and (C) shows exposures from 60 – 150 Lm.

83x125mm (300 x 300 DPI)

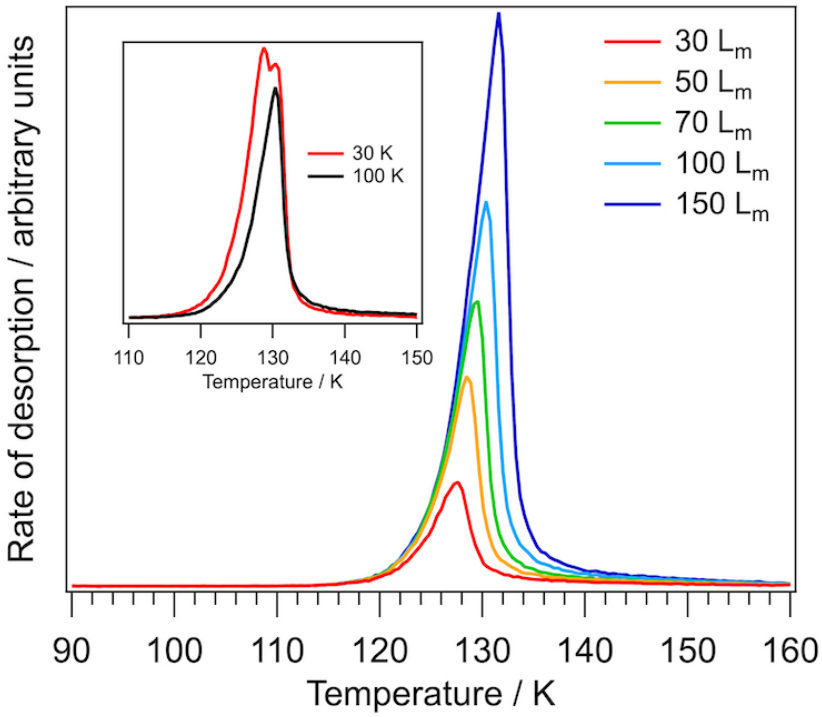

Figure 3: TPD data for a range of exposures of ethyl formate from 30 to 150 Lm following adsorption on HOPG at 100 K. The inset shows TPD spectra for 100 Lm of ethyl formate adsorbed at base temperature (30 K) and at 100 K.

76x57mm (300 x 300 DPI)

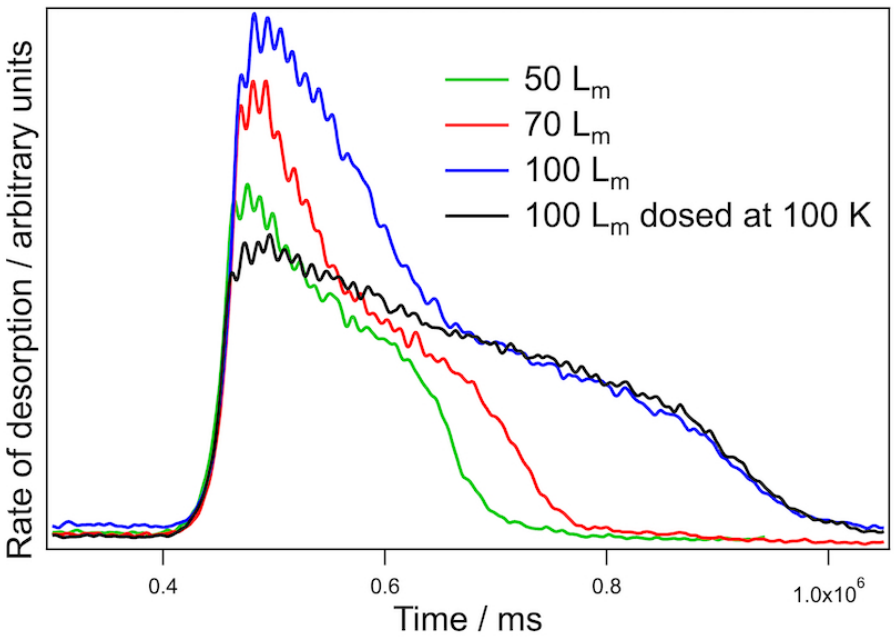

Figure 4: Isothermal desorption spectra recorded at 120 K for various exposures of ethyl formate adsorbed at 30 K (50, 70 and 100 Lm) and for 100 Lm ethyl formate adsorbed at 100 K.

76x51mm (300 x 300 DPI)

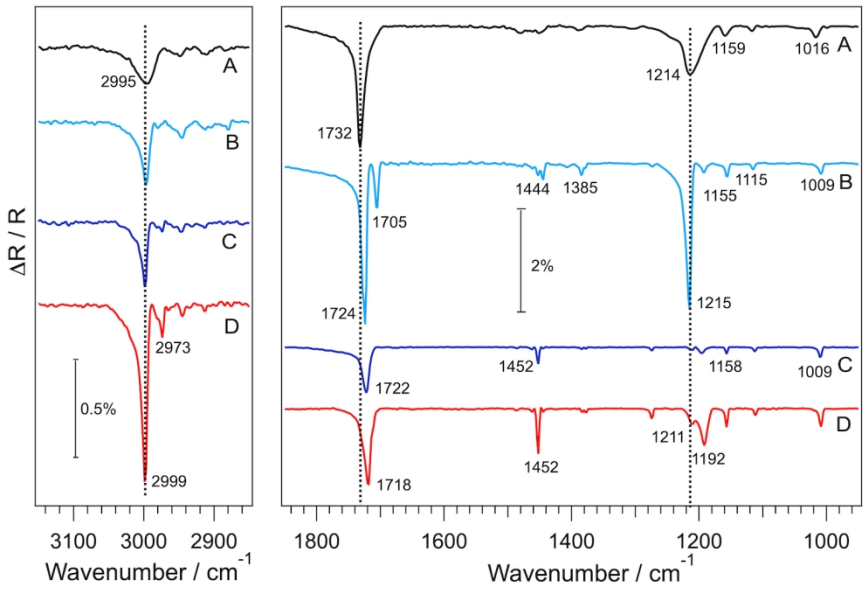

Figure 5: RAIR spectra of ethyl formate adsorbed on HOPG. (A) shows 100 Lm of ethyl formate adsorbed on HOPG at 30 K; (B) shows 100 Lm of ethyl formate annealed to 100 K;. (C) shows 100 Lm of ethyl formate annealed to 120 K; and (D) shows the spectrum for 100 Lm of ethyl formate adsorbed on HOPG at 100 K.

152x93mm (300 x 300 DPI)

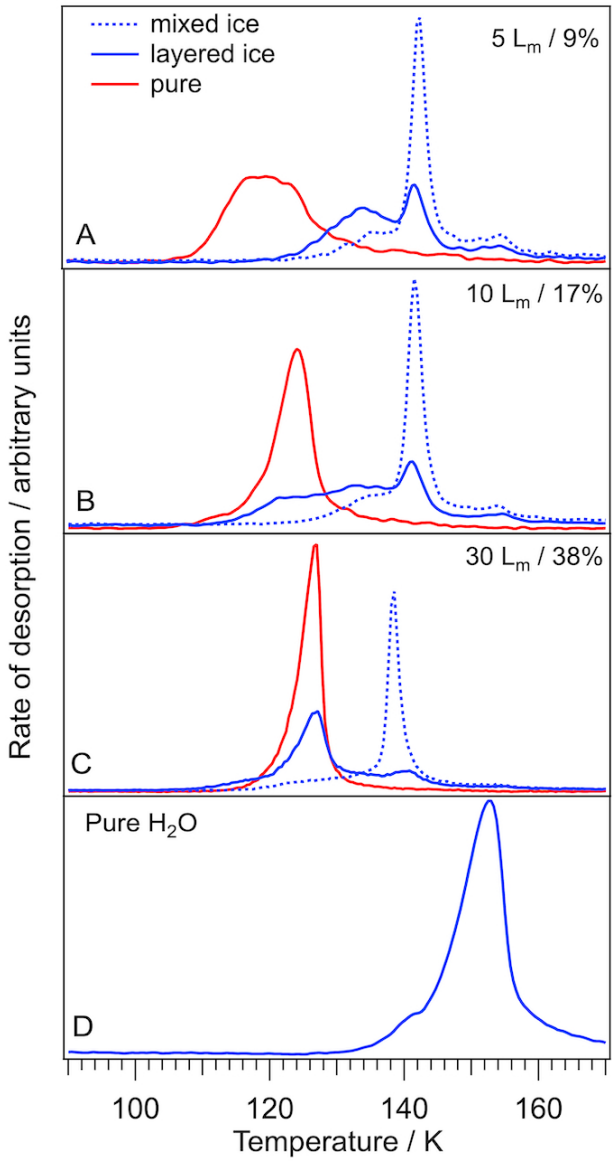

Figure 6: TPD traces for 5, 10 and 30 Lm of ethyl formate adsorbed on ASW in layered and mixed ices. (A) shows TPD spectra for 5 Lm (9%) of ethyl formate; (B) shows spectra for 10 Lm (17%) of ethyl formate; (C) shows spectra for 30 Lm (38%) of ethyl formate; and (D) shows a TPD spectrum for the desorption of a pure water ice layer adsorbed on HOPG at 30 K for comparison. In all cases the ASW exposure was 50 Lm.

81x112mm (300 x 300 DPI)

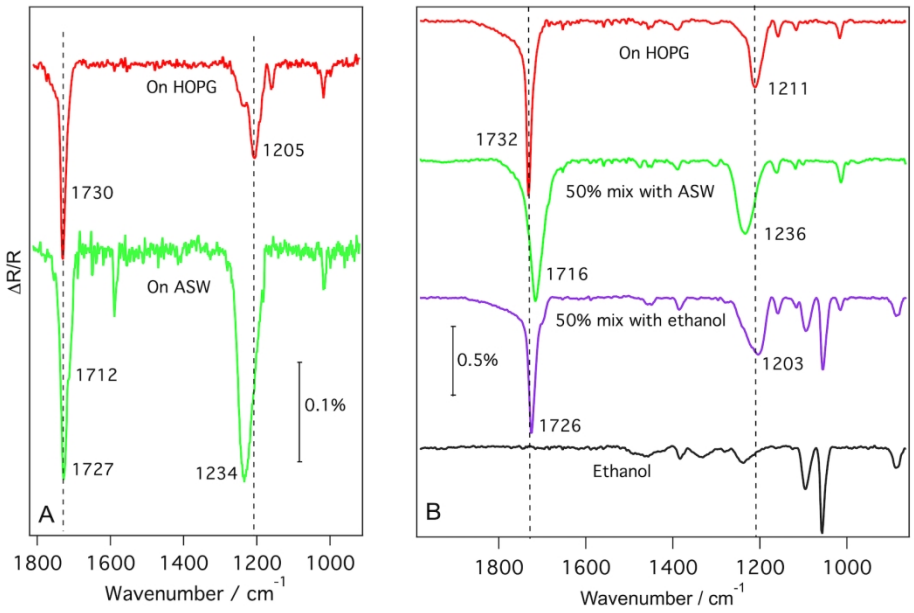

Figure 7: RAIR spectra for various ice configuratiions on HOPG. (A) Shows RAIR spectra for 10 Lm of ethyl formate adsorbed on HOPG at 30 K (top spectrum) and 10 Lm of ethyl formate adsorbed on top of 50 Lm of ASW at 30 K (bottom spectrum). (B) shows spectra for 50 Lm of ethyl formate adsorbed directly onto HOPG at 30 K, and in a 50% mix with ASW and ethanol at 30 K. The bottom spectrum shows a RAIR spectrum for 50 Lm of ethanol adsorbed on HOPG at 30 K.

165x104mm (300 x 300 DPI)

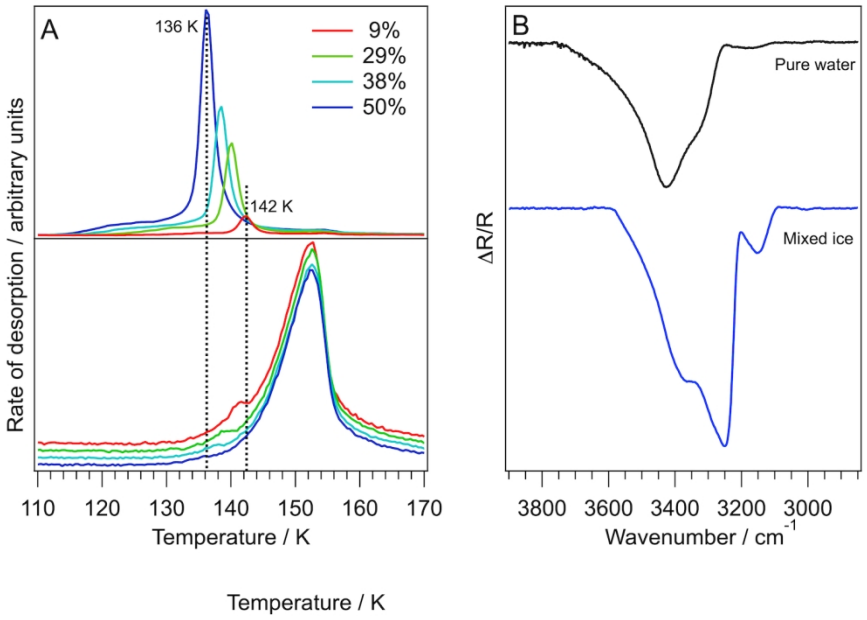

Figure 8: (A) TPD traces for ethyl formate and ASW mixtures of various compositions. The top spectra show the desorption of ethyl formate and the bottom spectra show the corresponding desorption of water. (B) Shows the O-H region of the RAIR spectrum for pure water adsorbed on HOPG and annealed to 130 K (top spectrum) and for a 50% ethyl formate/ASW mixture adsorbed at 30 K on HOPG and annealed to 130 K (bottom spectrum).

152x98mm (300 x 300 DPI)

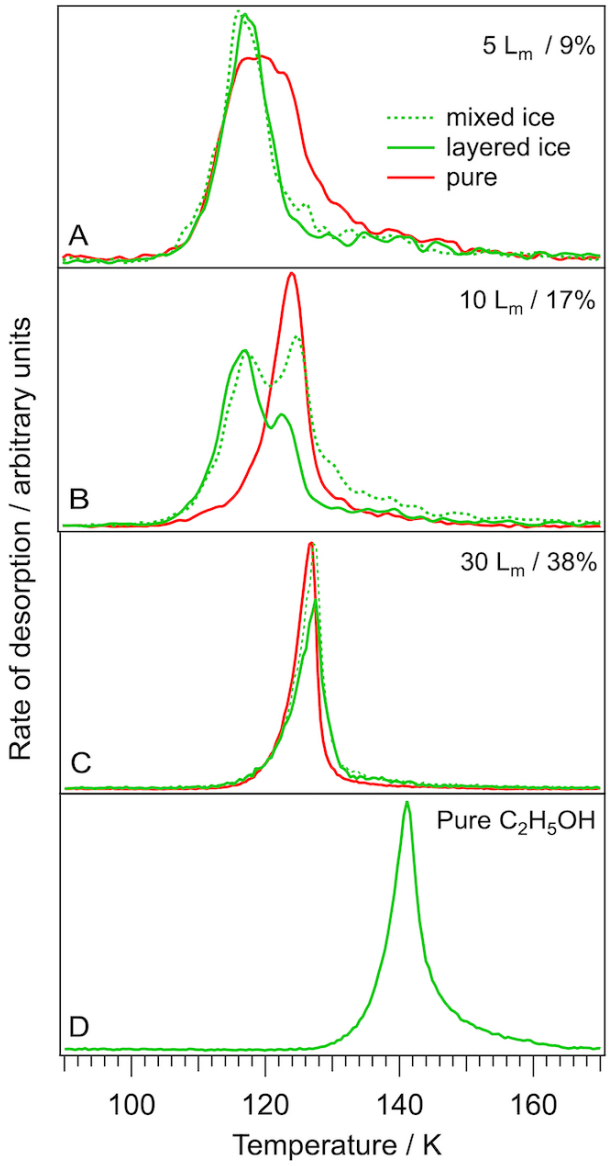

Figure 9: TPD traces for 5, 10 and 30 Lm of ethyl formate adsorbed on ethanol in layered and mixed ices. (A) shows TPD spectra for 5 Lm (9%) of ethyl formate; (B) shows spectra for 10 Lm (17%) of ethyl formate; (C) shows spectra for 30 Lm (38%) ethyl formate; and (D) shows a TPD spectrum for the desorption of an ethanol ice adsorbed on HOPG at 30 K for comparison. In all cases the ethanol exposure was 50 Lm.

81x110mm (300 x 300 DPI)